Development of an analytical simulation framework for angle-resolved photoemission spectra

M. Feidt,[1] S. Mathias,[2] and M. Aeschlimann[1]
[1]*Fachbereich Physik and Research Center OPTIMAS, Technische Universität Kaiserslautern, Erwin-Schrödinger-Str. 46, 67663 Kaiserslautern, Germany*
[2]*I. Physikalisches Institut, Georg-August-Universität Göttingen, Friedrich-Hund-Platz 1, 37077 Göttingen, Germany*

(Received 20 July 2017; revised manuscript received 19 May 2019; published 6 December 2019)

Angle-resolved photoemission spectroscopy (ARPES) is probably the most important experimental technique for the investigation of the electronic structure of solids. With respect to the interpretation of measured complex photoemission spectra, extensive theoretical efforts are often involved, as one needs a calculation of the band structure, a mapping of the band structure to the observed complex photoemission spectrum, and the inclusion of many-body effects. Typical methods that include the mentioned necessary steps for the interpretation are usually theoretically costly (such as time-dependent density functional theory). In contrast to purely numerical methods, analytical physical theories grant an easier approach in the implementation and, in general, allow for a more direct insight into the involved physical processes. Here, we show that combining a Keldysh Green's function formulation of the photoelectric current, together with a tight-binding parametrization of band structures, gives a powerful tool set for the simulation of ARPES spectra. Our approach is fast, capable of including many-body effects, and easy to be implemented and, therefore, from the viewpoint of an experimentalist, a valuable tool for the interpretation of photoemission spectra.

DOI: 10.1103/PhysRevMaterials.3.123801

I. INTRODUCTION

Nowadays, angle-resolved photoemission spectroscopy (ARPES) is by far the most important experimental technique to map the electronic structure of crystalline materials. The method played a key role in the determination of band structures and Fermi surfaces [1,2], in molecular orbital mapping [3], in the discovery and study of high-temperature superconductors [4,5] or topological insulators [6]. In order to be able to extract physical parameters from an ARPES spectrum, or to track changes in these by external parameter variations, a theoretical model of the system under investigation is needed. Today, sophisticated but highly numerical, theoretical methods based on time-dependent density functional theory (TDDFT) [7], density functional theory (DFT) [8], the Korringa-Kohn-Rostoker method (KKR) [9,10], or a nonequilibrium Keldysh formalism [11–14] are used for the interpretation of experimental photoemission data. But for a general understanding of a photoemission spectrum, it is often more useful to have an analytical model, capable of incorporating as many features as possible, but also being simple enough to be fast applicable and comprehensible. The focus of this paper is to provide a method for experimentalists which allows fast simulations for the interpretation and analysis of ARPES spectra without the need to be an expert on electronic structure theory.

For a complete theoretical modeling of an ARPES experiment (see Fig. 1), the band structure as well as the photoemission process itself, i.e., the creation of photohole-photoelectron pairs, has to be included in the calculations. Aside from the classic works on photoemission theory [15–21], based on standard perturbation theory, the most versatile approach capable of incorporating these requirements is the Keldysh formalism or real-time Green's function approach [22–24]. A straightforward formulation of one-photon photoemission within the Keldysh formalism has already been given by Caroli *et al.* [25]. Here, we extend their method by applying reasonable models for the treatment of the final and initial states and combine it with the combined interpolation scheme of Smith *et al.* [26,27], which allows to calculate the band structure of transition d-band metals. Our work combines known concepts and methods from photoemission theory and electronic structure theory in form of tight-binding models and compresses these to simplified but powerful formulas for the simulation of ARPES spectra. Although such an approach has been used extensively in the past [12,28,29], we focus on providing ready-to-use formulas for experimentalists.

These formulas, which by neglecting damping of the photoelectrons inside the solid, reduce to a fully analytical three-step model formula. Taking damping into account, bulk photoemission can be calculated with a single integral one-step model formula. In the context of our theory we discuss different spectral broadening mechanisms, a point which did not draw much attention in the past, review the lowest-order Feynman diagrams, and summarize the corresponding diagram rules to construct our ARPES formulas.

The paper is organized as follows: In Sec. II, we review the theory of Caroli *et al.* [25] and derive a generic formula for the photoelectric current. In Sec. III, we derive a set of Feynman rules, which can be used to construct photoemission formulas straight from a pictorial representation of the photoemission process [30–35], i.e., the corresponding Feynman diagram. In Secs. IV and V, we discuss specific models for the treatment of initial and final states and finally derive analytical results for the photoelectric current in Sec. VI, where the only undetermined quantities are the energy eigenvalues and the self-energies of final and initial states. A short discussion

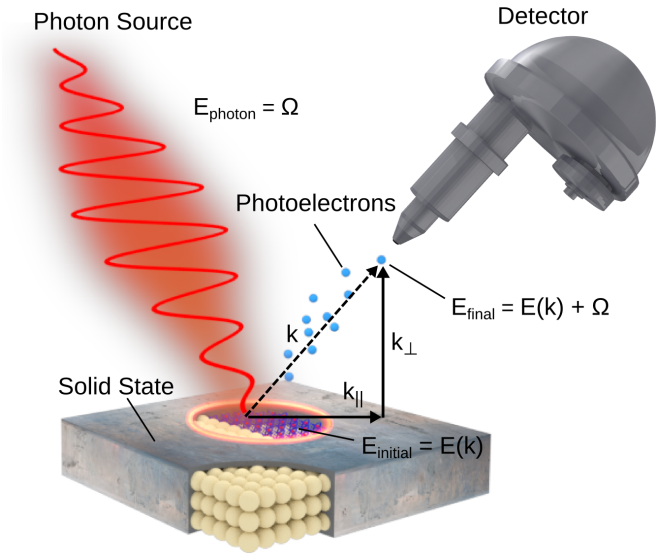

FIG. 1. Principle of angle-resolved photoemission spectroscopy.

follows on how our theoretical findings are related to the well-known one- and three-step-model descriptions of photoemission [18]. We present a first and simple simulation example in Sec. VII and discuss different spectral broadening mechanisms, followed by Sec. VIII, which deals with the inclusion of band structure information within the combined interpolation scheme. In Sec. IX, we present a comparison of theoretical simulations and experimental data for Ag(111) and Au(111) and give a short simulation guidance in Sec. X. Finally, the limitations of our modeling procedure are discussed in Sec. XI followed by a short summary and conclusion of our study in Sec. XII.

II. BASIC FORMALISM AND REVIEW OF ONE-PHOTON PHOTOEMISSION

Here, we briefly review the derivation of a general expression for the photoelectric current, up to second order in the interaction with an external light field. We start with the general Hamiltonian

$$H = H_0 + H_I, \tag{1}$$

where H_I denotes the light-matter interaction Hamiltonian

$$H_I = \int d^3r\, \hat{\psi}^\dagger(\mathbf{r},t)\left(\frac{ie\hbar}{m}\mathbf{A}(\mathbf{r},t)\nabla + \frac{e^2}{2m}\mathbf{A}^2(\mathbf{r},t)\right)\hat{\psi}(\mathbf{r},t). \tag{2}$$

The fermion field operators for electrons and holes can be expanded into eigenfunctions of the Hamiltonian H_0:

$$\begin{aligned}\hat{\psi}(\mathbf{r},t) &= \sum_n \hat{a}_{n,k}\phi_{n,k}(\mathbf{r})e^{-i\varepsilon_{n,\mathbf{k}}t},\\ \hat{\psi}^\dagger(\mathbf{r},t) &= \sum_n \hat{a}^\dagger_{n,k}\phi^*_{n,k}(\mathbf{r})e^{i\varepsilon_{n,\mathbf{k}}t},\end{aligned} \tag{3}$$

while $H_0\phi_{n,k} = E_{n,k}\phi_{n,k}$. Further, we assume that the eigenfunctions can be factorized in the form

$$\phi_{n,k}(\mathbf{r}) = \frac{1}{\sqrt{V}}u_{n,\mathbf{k}_\parallel}(\boldsymbol{\rho})e^{i\mathbf{k}_\parallel\cdot\boldsymbol{\rho}}\varphi_n(z) \tag{4}$$

with a lattice-periodic function $u_{n,\mathbf{k}_\parallel}(\boldsymbol{\rho})$, while $\boldsymbol{\rho} = (x,y)$ and z are the parallel and perpendicular lattice coordinates, respectively. Within the Keldysh formalism, the photoelectric current, in the plane parallel to the surface normal, can be calculated from the *lesser* Green's function $G^<$:

$$\mathbf{j}(\mathbf{r},t) = \frac{e\hbar}{m}(\nabla_{r'} - \nabla_r)G^<(\mathbf{r}t,\mathbf{r}'t)|_{\mathbf{r}'=\mathbf{r}=\infty} \tag{5}$$

[25]. The Keldysh Green's function satisfies the Dyson equation on the Keldysh contour [23]

$$\begin{aligned}G(x_1,x_2) &= G_0(x_1,x_2)\\ &\quad + \int dx_3 \int dx_4\, G_0(x_1,x_3)\Sigma(x_3,x_4)G(x_4,x_2),\end{aligned} \tag{6}$$

with $dx_i = d\mathbf{r}_i d\tau_i$, while Σ denotes the associated self-energy. The quantity G_0 is the corresponding Green's function to H_0, i.e., when all fields are turned off. If we turn on an external light field of the form

$$\mathbf{A}(t,\mathbf{r}) = \boldsymbol{\epsilon}A_0(z)\tilde{A}_L(t)\cos(\Omega t/\hbar), \tag{7}$$

where $\boldsymbol{\epsilon}$ is a polarization vector, Ω the photon energy, and $\tilde{A}_L(t)$ an envelope function, the associated self-energy is instantaneous and given by $\Sigma^\delta = \delta(x_1 - x_2)\mathbf{A}(t_1,\mathbf{r}_1)\nabla$. Here, we neglect the in-plane spatial extent of the light source, i.e., apply the dipole approximation but keep a formal z dependency, which will account later on for a finite penetration depth of the light source. For a continuous-wave light source (CW), we define $\tilde{A}_L(t) = 1$.

The diamagnetic part, proportional to $\mathbf{A}^2$, gives no contribution to the photoelectric current [25] in second order. Iterating Eq. (6) once, turning the contour integrals into integrals on the real axis and taking the "$<$" component [36], we get

$$\begin{aligned}&G^<(x_1,x_2)\\ &= G_0^<(x_1,x_2)\\ &\quad + \int dx_3 \int dx_4\, G_0^r(x_1,x_3)\Sigma^\delta(x_3,x_4)G^<(x_4,x_2)\\ &\quad + \int dx_3 \int dx_4\, G_0^<(x_1,x_3)\Sigma^\delta(x_3,x_4)G^a(x_4,x_2)\\ &\quad + \int dx_3 \int dx_4 \int dx_5 \int dx_6\, G_0^r(x_1,x_3)\Sigma^\delta(x_3,x_4)\\ &\quad \times G^<(x_4,x_5)\Sigma^\delta(x_5,x_6)G^a(x_6,x_2).\end{aligned} \tag{8}$$

The superscripts r and a denote the *retarded* and *advanced* Green's function. The relevant part of Eq. (8) for photoemission comes from the fourfold integral, which is of second order in $\mathbf{A}\cdot\nabla$, and therefore proportional to the intensity of the external field. Using the Bloch transformations

$$\begin{aligned}G(\mathbf{r}t,\mathbf{r}'t') &= \frac{1}{2\pi V}\sum_{n,\mathbf{k}_\parallel}\int d\omega\, G_{n,\mathbf{k}_\parallel,\omega}(z,z')\\ &\quad \times u_{n,\mathbf{k}_\parallel}(\boldsymbol{\rho})u^*_{n,\mathbf{k}_\parallel}(\boldsymbol{\rho}')e^{i\mathbf{k}_\parallel\cdot(\boldsymbol{\rho}-\boldsymbol{\rho}')}e^{-i/\hbar\,\omega(t-t')}\end{aligned} \tag{9}$$

and

$$\begin{aligned}j_{\mathbf{k}_\parallel,\omega,\omega'}(z,z') &= \sum_n \int dt \int d^2\rho \int dt' \int d^2\rho'\, j(\mathbf{r}t,\mathbf{r}'t)\\ &\quad \times u^*_{n,\mathbf{k}_\parallel}(\boldsymbol{\rho})u_{n,\mathbf{k}_\parallel}(\boldsymbol{\rho}')e^{-i\mathbf{k}_\parallel\cdot(\boldsymbol{\rho}-\boldsymbol{\rho}')}e^{i/\hbar(\omega t-\omega' t')},\end{aligned} \tag{10}$$

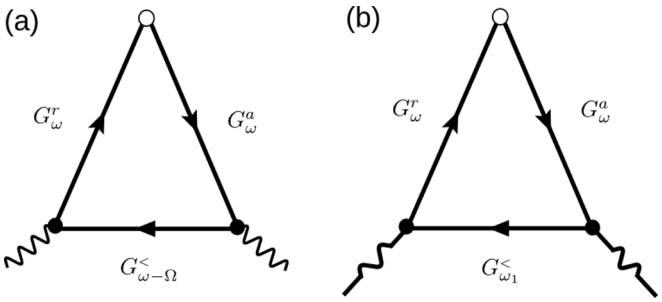

FIG. 2. Feynman diagrams for one-photon photoemission: (a) CW excitation, (b) laser pulse excitation.

and taking the z component of Eq. (5) we get the photoelectric current (perpendicular to the surface) for a CW source as a function of parallel momentum $\mathbf{k}_\parallel$ and binding energy ω (note that ω is defined as an energy and has units of eV):

$$j(\mathbf{k}_\parallel,\omega) = \frac{e\hbar}{m}\left(\frac{\partial}{\partial z'} - \frac{\partial}{\partial z}\right)\sum_{n,n'}|M_{nn'}|^2 \times \int dz_1 \int dz_2\, A_0(z_1)A_0(z_2) \times G^r_{n,\mathbf{k}_\parallel,\omega}(z,z_1)G^<_{n',\mathbf{k}_\parallel,\omega-\Omega}(z_1,z_2)G^a_{n,\mathbf{k}_\parallel,\omega}(z_2,z'). \tag{11}$$

Here, we imply the limit $z' = z = \infty$ and have taken the dc part of the photoelectric current, i.e., $\omega = \omega'$ [25]. Actually, the current would also contain a second term in Eq. (11), in which $\omega - \Omega$ is replaced by $\omega + \Omega$ for the lesser Green's function. However, this term is identical to zero, which follows from the general properties of the final and initial states [25]. The indices n and n' are labeling different bands in the band structure. The dipole matrix elements are given by

$$M_{nn'} = \frac{e\hbar}{m}\int \frac{d^2\boldsymbol{\rho}}{S_{1\,\mathrm{BZ}}}\, u^*_{n,\mathbf{k}_\parallel}(\boldsymbol{\rho})\boldsymbol{\epsilon}\cdot\nabla u_{n',\mathbf{k}_\parallel}(\boldsymbol{\rho}) \tag{12}$$

($S_{1\,\mathrm{BZ}}$ = area of the first Brillouin zone). Similar, for a pulsed laser source we get

$$j(\mathbf{k}_\parallel,\omega) = \frac{e\hbar}{m}\left(\frac{\partial}{\partial z'} - \frac{\partial}{\partial z}\right)\sum_{n,n'}|M_{nn'}|^2 \int dz_1 \int dz_2 \times \int d\omega'\, A_0(z_1)A_0(z_2)A_L^2[(\omega-\omega'-\Omega)/\hbar] \times G^r_{n,\mathbf{k}_\parallel,\omega}(z,z_1)G^<_{n',\mathbf{k}_\parallel,\omega'}(z_1,z_2)G^a_{n,\mathbf{k}_\parallel,\omega}(z_2,z'), \tag{13}$$

where $A_L(\omega)$ is the Fourier transform of $\tilde{A}_L(t)$.

III. FEYNMAN RULES FOR ARPES

What is left is now to specify the Green's functions $G^{r/a}$ and $G^<$ which will be described in the following sections. But, for the time being, we try to get an intuitive picture of the photoemission process described by Eq. (11) or (13). Therefore, we try to connect the mathematical expressions with a Feynman diagram representation of photoemission as shown in Fig. 2. In the photoemission process, the vector

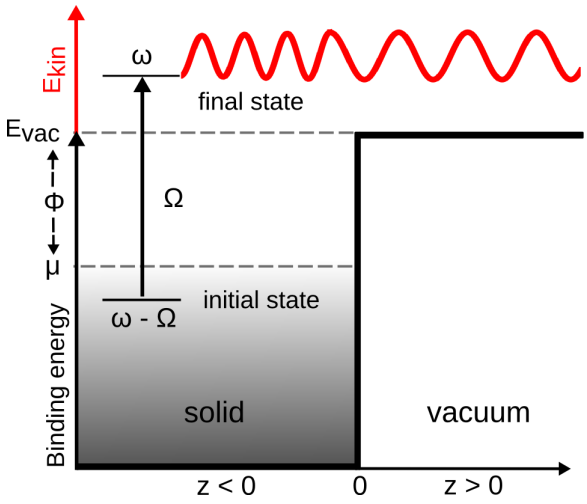

FIG. 3. Energy-level alignment for one-photon photoemission. The final state is represented by a matched free-electron state, damped inside the crystal but free in vacuum.

potential creates a photoelectron with energy ω by lifting electrons from an initial state into a final state propagating toward $z \to \infty$ (see Fig. 3). So, we identify the final state with $G^{r/a}_\omega$. But, this process leaves a hole behind in the crystal which has to be separated in energy from the final state by the amount Ω, i.e., the photon energy. Then, this hole has to be represented by the *lesser* function $G^<_{\omega-\Omega}$.

From this correspondence we can try to deduce some Feynman diagram rules, allowing us to directly translate the pictorial representation of Fig. 2 into a mathematical expression. The Feynman diagram rules for ARPES can be summarized as follows:

(1) To every fermion line, assign an energy and two spatial coordinates (perpendicular component), e.g., z and z'.

(2) $\mathbf{k}_\parallel$ is conserved for all fermion lines.

(3) A horizontal fermion line represents a photohole (excitation with $\omega < \mu$) $G^<$ [see Fig. 4(g)].

(4) A sloping line represents a final photoelectron state ($\omega > \mu$) $G^{r,a}$ [see Figs. 4(e) and 4(f)].

(5) Apply the following vertex rules:

(i) monochromatic photon source: apply the rules [Figs. 4(a) and 4(b)];

(ii) pulsed photon source: apply the rules [Figs. 4(c) and 4(d)].

(6) Integrate over all internal variables $\prod_{ij}\int d\omega_i \int dz_j$ (all variables excluding the final-state ones).

(7) Apply the current operator $e\hbar/m(\partial_{z'} - \partial_z)$ and take the limits $z \to z'$ and $\omega \to \omega'$ for the final-state variables at the apex [Fig. 4(h)].

Although these rules have only been derived from the lowest-order photoemission process (one-photon photoemission), also higher-order processes and photoemission formulas can be described and constructed from these rules.

IV. FINAL STATE

To get a more explicit expression for the photoelectric current, we have to apply a definite model for the final and initial states. For the final state we adopt the standard model

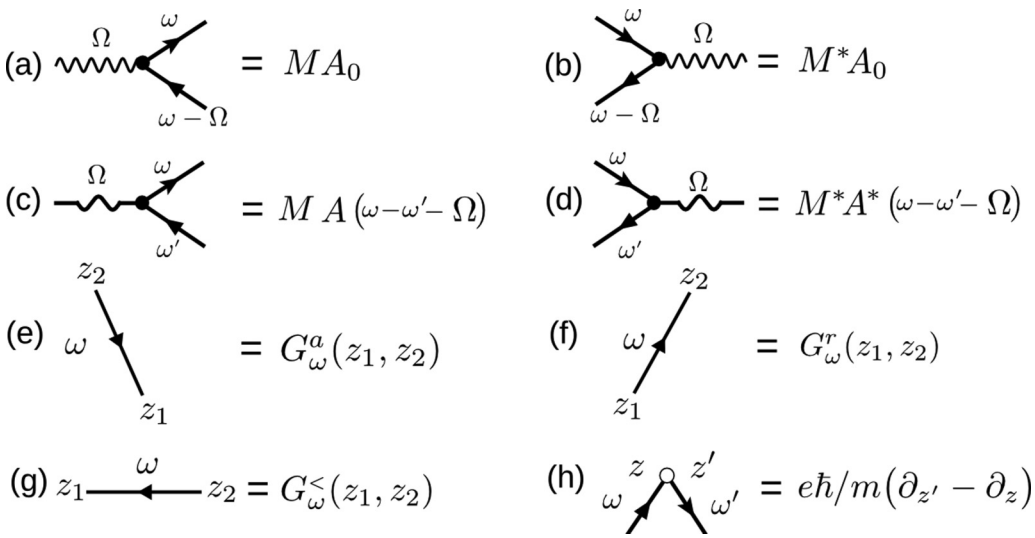

FIG. 4. Feynman rules for photoemission.

of an electron trapped in a semi-infinite step surface potential well, representing the crystal. Outside the potential well, the electron is assumed to be free. In general, this type of final state is known as a time-reversed low-energy electron diffraction (LEED) state, when the asymptotically free wave function is matched to the real crystal potential [15,17,18]. As long as we are not interested in photoemission from states whose wave functions are considerably extended outside the crystal, e.g., image potential states, the main contribution of the photocurrent comes from the integral region inside the crystal, so that we only need the final-state Green's function

$$G^r_{\mathbf{k}_\parallel,\omega}(z,z') = -\frac{2mi}{\hbar^2}\frac{e^{i(k_v z - k_s z')}}{k_v + k_s}, \quad z>0,\ z'<0 \tag{14}$$

$$G^a_{\mathbf{k}_\parallel,\omega}(z,z') = \frac{2mi}{\hbar^2}\frac{e^{-i(k_v z - k_s z')}}{k_v + k_s}, \quad z>0,\ z'<0 \tag{15}$$

which one gets after matching the potential well solutions outside and inside the crystal [25]. The perpendicular momentum inside the crystal can be split into real and imaginary parts, i.e., $k_s = k_{\mathrm{sr}} + ik_{\mathrm{si}}$ so that

$$k_v = \left(\frac{2m}{\hbar^2}[\omega - \varepsilon_{\mathbf{k}_\parallel} - E_{\mathrm{vac}}]\right)^{1/2}, \tag{16}$$

$$k_{\mathrm{sr}} = \mathrm{Re}\left(\frac{2m}{\hbar^2}[\omega - \varepsilon_{\mathbf{k}_\parallel} - \Sigma^r(\omega)]\right)^{1/2}, \tag{17}$$

$$k_{\mathrm{si}} = \mathrm{Im}\left(\frac{2m}{\hbar^2}[\omega - \varepsilon_{\mathbf{k}_\parallel} - \Sigma^r(\omega)]\right)^{1/2}, \tag{18}$$

with $E_{\mathrm{vac}} = \mu + \Phi$, where Φ denotes the work function and $\varepsilon_{\mathbf{k}_\parallel} = \hbar^2\mathbf{k}_\parallel^2/2m$. The energy-dependent retarded self-energy $\Sigma^r(\omega)$ accounts for possible losses inside the solid. In addition, the final state has to fulfill the condition

$$G^{r/a}_{\mathbf{k}_\parallel,\omega}(z,z') \propto \theta(\omega - \varepsilon_{\mathbf{k}_\parallel} - E_{\mathrm{vac}}), \tag{19}$$

reflecting the requirement of a positive transversal energy of the final-state photoelectron. This property generates the exit cone in the final ARPES spectrum.

V. INITIAL STATE

The initial state enters the photoelectric current (11) via the *lesser* Green's function which is connected to the retarded Green's function and the spectral function $A(\mathbf{k}_\parallel, k_z, \omega)$ by

$$\begin{aligned} G^<_{\mathbf{k},\omega} &= -2i\,\mathrm{Im}\,G^r_{\mathbf{k},\omega} f(\omega-\mu) \\ &= iA(\mathbf{k},\omega) f(\omega-\mu), \end{aligned} \tag{20}$$

where f is the Fermi distribution and μ the Fermi energy ($\mathbf{k} = (\mathbf{k}_\parallel, k_z)$). In the noninteracting case, the spectral function is given by

$$A(\mathbf{k},\omega) = 2\pi\delta(\omega - \epsilon_{\mathbf{k}} + \mu). \tag{21}$$

As soon as interactions, such as electron-electron, electron-phonon, or electron-impurity scattering, are taken into account, the sharp energy eigenvalues $\varepsilon_{\mathbf{k}}$ are turned into a spectral distribution

$$A_n(\mathbf{k},\omega) = \frac{-2\,\mathrm{Im}\Sigma^r_{\mathbf{k},\omega}}{\left(\omega - \epsilon_{n,\mathbf{k}} + \mu - \mathrm{Re}\Sigma^r_{\mathbf{k},\omega}\right)^2 + \left(\mathrm{Im}\Sigma^r_{\mathbf{k},\omega}\right)^2}, \tag{22}$$

where we introduced in addition a band index n. In the following, we propose three simple approximations which will allow us to derive analytical expressions for the photoelectric current (11), including photoemission from bulk states, localized states and $2d$ states.

A. Bulk states

For the case of valence band photoemission from metal bulk bands we approximate the z-dependent part of the wave function with [37]

$$\varphi_{k_z}(z) \sim \sin(k_z z + \delta), \tag{23}$$

where δ is usually an energy- and momentum-dependent function. Starting from the $\mathbf{k}$-dependent *lesser* Green's function (20) and expanding in terms of the wave functions (23), we can derive the function

$$\begin{aligned} G^<_{n,\mathbf{k},\omega}(z_1,z_2) = 2\pi i \int dk_z \sin(k_z z_1 + \delta)\sin(k_z z_2 + \delta) \\ \times A_n(\mathbf{k},\omega) f(\omega-\mu). \end{aligned} \tag{24}$$

B. Localized bulk states

The lesser function for the localized case is calculated by assuming a completely localized initial-state wave function with binding energy ε_n, and summing over an infinite layer of lattice planes at a distance $a_j - a_{j-1}$:

$$\begin{aligned} &G^<_{n,\mathbf{k},\omega}(z_1, z_2) \\ &= 2\pi i \sum_j \delta(z_1 - a_j)\delta(z_2 - a_j)\delta(\omega - \varepsilon_n) f(\omega - \mu) \\ &= 2\pi i\, \delta(z_1 - z_2)\delta(\omega - \varepsilon_n) f(\omega - \mu) \\ &= i\, \delta(z_1 - z_2) A_n^{loc}(\omega) f(\omega - \mu). \end{aligned} \tag{25}$$

Note that the Green's function (25) is independent of $\mathbf{k}$.

C. 2d states

To describe surface states, interface states, or true $2d$ states of materials like graphene we make the rough approximation of a completely localized state at depth z_0:

$$\begin{aligned} &G^<_{n,\mathbf{k},\omega}(z_1, z_2) \\ &= 2\pi i\, \delta(z_1 - z_0)\delta(z_2 - z_0)\, \delta(\omega - \varepsilon_{n,\mathbf{k}_\parallel}) f(\omega - \mu) \\ &= i\, \delta(z_1 - z_0)\delta(z_2 - z_0)\, A_n^{2d}(\mathbf{k}_\parallel, \omega) f(\omega - \mu). \end{aligned} \tag{26}$$

VI. ANALYTICAL EXPRESSIONS FOR THE PHOTOCURRENT

Now that we specified definite models for the final and initial states, we can solve the integrals in Eq. (11). We neglect the spatial dependency of the vector potential in the sample plane but take a finite penetration depth of the light field into account by assuming an exponential decay $A(z) = A_0 e^{z/2l_p}$, where l_p denotes the penetration depth of the vector potential. If we then plug Eqs. (14) and (15) into Eq. (11), symmetrize by using the fact that Eq. (11) is symmetric under the interchange of z_1 and z_2, and change to kinetic energy $E = E_{\mathrm{kin}} = \omega - E_{\mathrm{vac}}$, we get

$$\begin{aligned} j_{pes}(\mathbf{k}_\parallel, E) = &- \sum_n \left(\frac{2iem}{\hbar}\right) |M_n|^2 A_0^2\, \theta(E - \varepsilon_{\mathbf{k}_\parallel}) \\ &\times \int_{-\infty}^{0} dz_1 \int_{-\infty}^{0} dz_2\; G^<_{n,\mathbf{k}_\parallel, E-\Omega}(z_1, z_2) \\ &\times \frac{k_v \cos[k_{\mathrm{sr}}(z_1 - z_2)]}{(k_v + k_{\mathrm{sr}})^2 + k_{\mathrm{si}}^2} e^{(k_{\mathrm{si}} + 1/2l_p)(z_1 + z_2)}. \end{aligned} \tag{27}$$

We start with the photocurrent for bulk photoemission. Insertion of the Green's function (24) into (27) results into

$$\begin{aligned} j_{\mathrm{pes}}(\mathbf{k}_\parallel, E) = &\sum_n \left(\frac{2em}{\hbar}\right) |M_n|^2 A_0^2\; f(E - \Omega + \Phi) \\ &\times \theta(E - \varepsilon_{\mathbf{k}_\parallel}) \int dk_z\; \frac{k_v}{(k_v + k_{\mathrm{sr}})^2 + k_{\mathrm{si}}^2} \\ &\times K(\mathbf{k}_\parallel, k_z, E) A_n(\mathbf{k}_\parallel, k_z, E - \Omega), \end{aligned} \tag{28}$$

where $k_L = k_{\mathrm{si}} + 1/2l_p$. We have introduced the photoemission kernel function (and neglected δ)

$$K(\mathbf{k}_\parallel, k_z, E) = \frac{k_z^2}{k_L^4 + \left(k_{\mathrm{sr}}^2 - k_z^2\right)^2 + 2k_L^2\left(k_{\mathrm{sr}}^2 + k_z^2\right)}, \tag{29}$$

which weights the contribution of the spectral function to the total photocurrent in momentum and energy. The calculation of the photocurrent is now reduced to a single integral. The only functions which are still undetermined are the eigenvalue spectrum of the initial state, i.e., $\varepsilon_{n,\mathbf{k}}$, and the self-energies for the initial and final states. If we neglect final-state damping, i.e., k_L, in the kernel K we can simplify Eq. (28) further. Then, K is only large for $k_{\mathrm{sr}}^2 \approx k_z^2$, so we can replace K by

$$K \approx \delta\left(k_{\mathrm{sr}}^2 - k_z^2\right) = \frac{1}{2|k_{\mathrm{sr}}|}[\delta(k_z - k_{\mathrm{sr}}) + \delta(k_z + k_{\mathrm{sr}})]. \tag{30}$$

Since only the first part of Eq. (30) can lead to photoemission in the forward direction, Eq. (28) turns into

$$\begin{aligned} j_{\mathrm{pes}}^{\mathrm{bulk}}(\mathbf{k}_\parallel, E) = &\sum_n \left(\frac{em}{\hbar}\right) |M_n|^2 A_0^2 \frac{k_v}{|k_{\mathrm{sr}}|} \frac{\theta(E - \varepsilon_{\mathbf{k}_\parallel})}{(k_v + k_{\mathrm{sr}})^2 + k_{\mathrm{si}}^2} \\ &\times f(E - \Omega + \Phi) A_n^{\mathrm{bulk}}(\mathbf{k}_\parallel, k_z, E - \Omega)|_{k_z = k_{\mathrm{sr}}} \end{aligned} \tag{31}$$

with

$$k_{\mathrm{sr}} = \mathrm{Re}\left(\frac{2m}{\hbar^2}[E + V_0 - \varepsilon_{\mathbf{k}_\parallel} - \Sigma^r(\omega)]\right)^{1/2}. \tag{32}$$

Note that we have replaced E_{vac} with V_0, often termed the inner potential, which we leave as an adjustable parameter and absorbed the factor $(2em/\hbar)$ into the definition of the dipole matrix element.

For a pulsed laser source one obtains

$$\begin{aligned} j_{\mathrm{pes}}^{\mathrm{bulk}}(\mathbf{k}_\parallel, E) = &\sum_n |M_n|^2 A_0^2 \frac{k_v}{|k_{\mathrm{sr}}|} \frac{\theta(E - \varepsilon_{\mathbf{k}_\parallel})}{(k_v + k_{\mathrm{sr}})^2 + k_{\mathrm{si}}^2} \\ &\times \int dE' A_L^2(E - E' - \Omega) f(E' + \Phi) \\ &\times A_n^{\mathrm{bulk}}(\mathbf{k}_\parallel, k_z, E')\Big|_{k_z = k_{\mathrm{sr}}}. \end{aligned} \tag{33}$$

The interpretation of Eqs. (31) and (33) is straightforward. Due to energy and momentum conservation the photoelectric current is given by the intersection of a free-electron parabola and the spectral function of the initial state [see Fig. 5(b)]. While $\mathbf{k}_\parallel$ is completely preserved, the cut in k_z depends on the photon energy Ω.

Similar formulas can be calculated for the remaining two cases. For two-dimensional initial states, we get

$$\begin{aligned} j_{\mathrm{pes}}^{2d}(\mathbf{k}_\parallel, E) = &\sum_n |M_n|^2 A_0^2 \frac{k_v\, \theta(E - \varepsilon_{\mathbf{k}_\parallel})}{(k_v + k_{\mathrm{sr}})^2 + k_{\mathrm{si}}^2} \\ &\times f(E - \Omega + \Phi) A_n^{2d}(\mathbf{k}_\parallel, E - \Omega)\, e^{-2k_L|z_0|}. \end{aligned} \tag{34}$$

In contrast to the bulk case [Eq. (31)], the dispersion of the initial state does not depend on the wave vector of the final state k_{sr} and, therefore, is independent of the photon energy

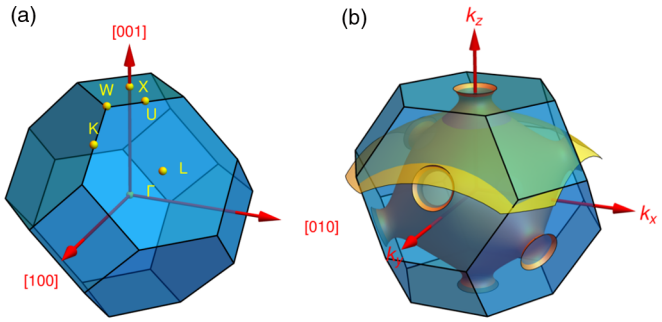

FIG. 5. (a) The fcc Brillouin zone with high-symmetry points. (b) Schematic cut through the constant energy surface of the initial state (orange). The plane (yellow) corresponds to the free-electron final state, while the relative position of the plane to the initial state depends on the photon energy.

Ω. For localized initial states we get the current

$$j^{loc}_{\rm pes}(\mathbf{k}_\parallel, E) = \sum_n |M_n|^2 A_0^2 \frac{1}{k_L} \frac{k_v\,\theta(E-\varepsilon_{\mathbf{k}_\parallel})}{(k_v+k_{\rm sr})^2+k_{\rm si}^2} \times f(E-\Omega+\Phi) A_n^{loc}(E-\Omega), \quad (35)$$

where the initial state does not have any dispersion at all.

The final approximation we will make use of for all simulations which will follow is to treat the dipole matrix elements M_n as constants. Such an approximation allows the photocurrent contribution to vary for individual band transitions but does not introduce additional structure in the ARPES band dispersions.

A. Recovery of the three-step model

We now compare our bulk photoemission formula to the angle-resolved formula of Feibelman and Eastman [18]. They have shown how the photocurrent derived by Caroli *et al.* [25] can be converted to a Fermi's golden rule type formula of photoemission and demonstrated the equivalence of these formulations for an independent electron solid. Further, they have shown that within a small $k_{\rm si}$ approximation, i.e., $zk_{\rm si} \ll 1$, where z is the distance, the final-state electron is traveling through the crystal, the photocurrent turns into a three-step-model formula. Their formula can be summarized as

$$j(\mathbf{k}, E) \propto \sum_n |M_n|^2 A_0^2\, |T|^2 \frac{1}{k_{\rm si}} \delta(k_{\rm sr}-k_z)\theta(E-\varepsilon_{\mathbf{k}_\parallel}) \times \delta(E-\Omega-E_{\mathbf{k},n}). \quad (36)$$

Here, T_n is an expansion coefficient resulting from a linear expansion of the final state into products of an in-plane periodic Bloch function and a plane wave for the out-of-plane component matched at the surface of the solid, so as we did. $E_{\mathbf{k},n}$ is the initial-state energy. Up to a minor difference, we end up with the same result [Eqs. (28) and (31)]

$$j(\mathbf{k}, E) \propto \sum_n |M_n|^2 A_0^2 \frac{k_v}{(k_v+k_{\rm sr})^2+k_{\rm si}^2} \frac{1}{k_{\rm sr}} \theta(E-\varepsilon_{\mathbf{k}_\parallel}) \times \delta(k_{\rm sr}-k_z)\, A_n^{\rm bulk}(\mathbf{k}_\parallel, k_z, E-\Omega). \quad (37)$$

That means our kernel approximation [Eq. (30)] splits the photocurrent into a product of terms describing photoemission as a three-step process. Photoexcitation is described by the term $|M_n|^2 A_n^{\rm bulk}$, which would equal the last energy delta function of Eq. (36) for a noninteracting solid. In contrast to Feibelman and Eastman we made the approximation of a completely vanishing damping of the final state in the kernel function and get a factor $1/k_{\rm sr}$ while they get a factor $1/k_{\rm si}$ describing propagation to the surface. Finally, in our case the transmission coefficient $|T|^2$ is given by $k_v/[(k_v+k_{\rm sr})^2 + k_{\rm si}^2]$.

B. The need for a one-step-model description

The photocurrent formulas we presented exhibit four sources of spectral broadening. The first two are final-state scattering, included via Σ^r, and a finite penetration depth l_p of the used light source, both leading to a finite $k_{\rm si}$. Further, we have the initial-state spectral width and a possible spectral width for a pulsed laser source. The effect of these on the final photoemission signal will be discussed in more detail in the next section. Without neglecting final-state damping in the kernel function, the photocurrent can not be separated into terms carrying information about the solid and the surface solely. In this case, the delta function (30) is not valid anymore and one has to use the one-step formula. In particular, taking final-state broadening into account, one has to use Eq. (28) to describe the effect of the final-state losses on the spectral width of the measured photoemission signal which sets already the limit for the use of the three-step model.

VII. A FIRST EXAMPLE

As a first simulation example, and to show what the theory presented so far is capable of, we calculate photoemission spectra for the case of bulk photoemission. Let us assume we have a material with a face-centered-cubic (fcc) structure [see Fig. 5(a)]. With a simple tight-binding model we can calculate the energy of a single conduction band by

$$\varepsilon_{\mathbf{k}} = \varepsilon_0 + V \sum_n e^{i\mathbf{k}\mathbf{R}_n}, \quad (38)$$

i.e., by a superposition of simple plane-wave states. The sum in (38) runs over all 12 nearest neighbors given by the coordinate set $a/2(\pm1, \pm1, 0)$, $a/2(\pm1, 0, \pm1)$, $a/2(0, \pm1, \pm1)$, where a is a lattice constant. So, we obtain

$$\varepsilon_{\mathbf{k}} = \varepsilon_0 + 4V\left[\cos\left(\frac{k_x a}{2}\right)\cos\left(\frac{k_y a}{2}\right) + \cos\left(\frac{k_x a}{2}\right)\cos\left(\frac{k_z a}{2}\right) + \cos\left(\frac{k_y a}{2}\right)\cos\left(\frac{k_z a}{2}\right)\right]. \quad (39)$$

Now, we use the quasiparticle spectral function (22) and Eq. (39) to obtain

$$A(\mathbf{k}, \omega) = \frac{2\Gamma}{(\omega-\varepsilon_{\mathbf{k}}+\mu)^2+\Gamma^2}, \quad (40)$$

assume $\Gamma = -{\rm Im}\Sigma^r_{\mathbf{k},\omega}$ to be constant, and the real part of the self-energy to be zero. If we then plug the spectral function (40) into the formula for bulk photoemission (31), we can

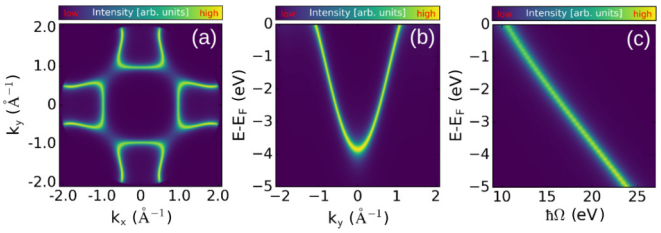

FIG. 6. (a) Momentum map at $E - E_f = -0.5$ eV, $\Omega = 21$ eV, (b) binding energy vs parallel momentum map with $\Omega = 21$ eV, (c) binding energy vs photon energy for $k_{||} = 0$.

simulate photoemission spectra as a function of

(i) k_x, k_y with $E = \text{const}$ [see Fig. 6(a)];

(ii) $E, \mathbf{k}_{||}$ [see Fig. 6(b)];

(iii) E, Ω while $\mathbf{k}_{||} = \text{const}$ [see Fig. 6(c)].

We used a photon energy of 21 eV corresponding to a He discharge lamp, a standard UV low-bandwidth light source used for ARPES.

A. Spectral broadening mechanisms

Using the same model (39) but rotated to the [111] crystal direction, as described in Sec. VIII, we calculate difference momentum maps by subtracting the spectrum one gets when only taking initial-state broadening into account [Fig. 7(a)] using Eq. (31) from a spectrum with an additional broadening mechanism. All spectra [Figs. 7(a)–7(d)] have been normalized in the intensity range [0,1] before the subtraction. For the initial state we use a constant purely imaginary self-energy $\Gamma = 150$ meV. We start with the effect of final-state broadening [Fig. 7(b)] and now use Eq. (28). We set the spectral width of the final state to a constant value of 2 eV which corresponds to a lower realistic limit for noble-metal excited states in the energy region of ∼20 eV [38].

Second, we are using Eq. (33) with a laser envelope function $A_L(E - \Omega) = \text{sech}[(E - \Omega)/\Delta\omega]$. We set the photon energy Ω to 22 eV and the spectral width $\Delta\omega$ to 150 meV which are realistic values for a high harmonic generation light source used for ARPES [39] [Fig. 7(c)].

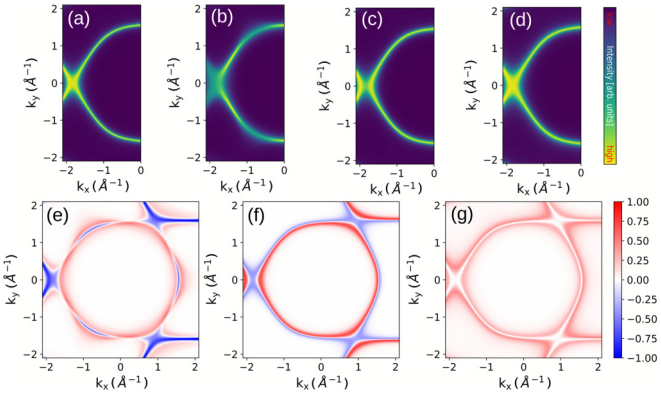

FIG. 7. Momentum maps with spectral broadening including only the initial-state self-energy (a), plus final-state broadening (b), plus laser source (c), plus finite penetration depth (d), (e)–(g) difference plots where we subtracted (a) from (b), (c), (d), respectively

Finally, we combine Eq. (28) with a finite penetration depth l_p. Using optical data from [40] we can calculate the extinction coefficient for, e.g., Ag at 22 eV, $\kappa = \text{Im}\sqrt{\epsilon_1 + i\epsilon_2} = 0.752$, so that $l_p = \hbar c_0/\Omega 2\kappa = 6.247$ nm [Fig. 7(d)].

The laser broadening [Fig. 7(c)] leads just to a small uniform blurring of the measured band structure, as one would expect because A_L does not depend on momentum, and a shift of the transition resonance toward higher energies. In the difference plot [Fig. 7(f)], this leads to an increase of intensity on the inner side of the cone and a decrease on the outer side of the cone as the the measured band dispersion depends on the photon energy. The effect of a finite final-state lifetime is much more prominent [Figs. 7(b) and 7(e)]. This effect leads to an additional structure in the momentum distribution because the resonance condition for a band transition is now altered by the photoemission kernel [Eq. (29)] and a momentum dependent k_{si}. In case of a finite penetration depth [Fig. 7(g)], which enters the kernel function as a constant, we find the overall linewidth again just smeared out.

VIII. INCLUDING THE BAND STRUCTURE

The energy eigenvalues $\varepsilon_{\mathbf{k}}$ in (22) depend on many parameters such as the crystal structure, the orbital character of the involved electrons, and of course on the interactions between the electrons. To simplify matters and approximating the band structure of a material, so-called combined-interpolation schemes have been developed, pioneered by Fletcher, Hodges, Ehrenreich, Lang, and Mueller [41–43]. The principle of band structure interpolation schemes is the following: first one uses a first-principles method to calculate the band structure of a material. Then, a suitable parametrization is used in the formulation of a tight-binding Hamiltonian, while using an appropriate basis set of eigenfunctions. The parameters of the model are then adjusted to match the band structure of the full calculation.

We adapt the extended band structure interpolation scheme of Smith [27] for transition d-band metals. Note that this model is a pure bulk band model which assumes a perfect three-dimensional (3D) crystal. Therefore, the model does not involve surface states. The scheme combines the d-band parametrization of Fletcher [41] and extends the sp-band parametrization of Mueller [43], as well as the Hodges-Ehrenreich-Lang scheme [42]. Details about the implementation can be found in the listed references. The used model Hamiltonian is given by

$$H(k_x, k_y, k_z) = \begin{pmatrix} H_{cc} & H_{cd} & 0 & 0 \\ H_{dc} & H_{dd} + \xi M & 0 & \xi N \\ 0 & 0 & H_{cc} & H_{cd} \\ 0 & -\xi N^* & H_{dc} & H_{dd} + \xi M^* \end{pmatrix}. \tag{41}$$

H_{cc}, H_{dd}, and H_{cd} (H_{dc}) represent a 15 × 15 orthogonalized plane-wave block for the sp bands, a 5 × 5 d-band block, and a 15 × 5 block describing the hybridization between the sp and d bands. In contrast to [27], we exclude the single k vector $(2\pi/a)(-2, -2, 0)$ which would lead to asymmetric photoemission spectra. Spin-orbit coupling is included via the matrices M and N and the spin-orbit coupling parameter ξ. The energy eigenvalues are then obtained by solving the

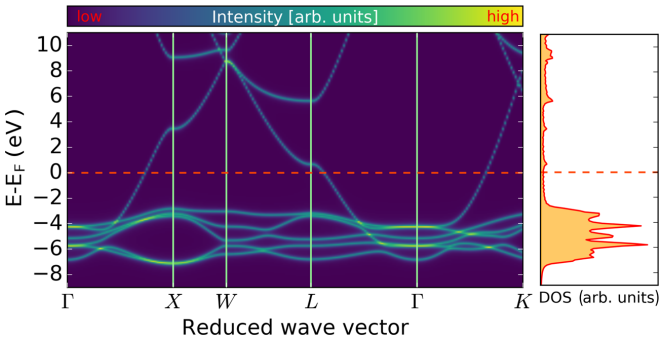

FIG. 8. Calculated spectral function of Ag along high-symmetry directions, $\Gamma = 0.4$ eV, using with the combined interpolation scheme with the parameter set of [44].

characteristic equation

$$|H(k_x, k_y, k_z)_{ij} - \varepsilon_{i,\mathbf{k}}\,\delta_{ij}| = 0, \tag{42}$$

leading to 40 energy bands $\varepsilon_{n,\mathbf{k}}$ with $n = 1, \ldots, 40$. If we do not include electron interactions which go beyond the first-principles calculation, we can again simply turn the eigenvalues into a spectral function

$$A_n(\mathbf{k}, E) = \frac{2\Gamma}{(E - \varepsilon_{n,\mathbf{k}} + \mu)^2 + \Gamma^2}, \tag{43}$$

by making again the simplest possible approximation for $\Sigma^r_{\mathbf{k},E}$, i.e., $\mathrm{Re}\Sigma^r_{\mathbf{k},E} = 0$, while the imaginary part of the self-energy is just a constant, $\mathrm{Im}\Sigma^r_{\mathbf{k},E} = -\Gamma$, turning the sharp bands into quasiparticles (see Fig. 8).

IX. SIMULATION OF ARPES SPECTRA AND COMPARISON WITH EXPERIMENTAL DATA

To be able to apply the combined interpolation scheme from Sec. VIII to the [111] direction, we have to rotate the momentum vectors by

$$\begin{pmatrix} k'_x \\ k'_y \\ k'_z \end{pmatrix} = \begin{pmatrix} \cos\alpha & -\sin\alpha & 0 \\ \sin\alpha & \cos\alpha & 0 \\ 0 & 0 & 1 \end{pmatrix} \times \begin{pmatrix} \cos\beta & 0 & \sin\beta \\ 0 & 1 & 0 \\ -\sin\beta & 0 & \cos\beta \end{pmatrix} \begin{pmatrix} k_x \\ k_y \\ k_z \end{pmatrix}, \tag{44}$$

where $\alpha = \pi/4$ and $\beta = \arccos(1/\sqrt{3})$, so that the z component of the momentum vector points into the [111] direction because the energy eigenvalue calculation is formulated in a coordinate system with $k_z \parallel [001]$ (see Fig. 5). Using the new momentum vectors

$$k'_x = k_x \cos\alpha \cos\beta - k_y \sin\alpha + k_z \cos\alpha \sin\beta, \tag{45}$$

$$k'_y = k_y \cos\alpha + k_z \sin\alpha \sin\beta + k_x \sin\alpha \cos\beta, \tag{46}$$

$$k'_z = k_z \cos\beta - k_x \sin\beta, \tag{47}$$

we calculate ARPES spectra and momentum maps for a photon energy of 21.2 eV for Ag(111). In Fig. 9 we present cuts along $W - \Gamma - W$ and $L - \Gamma - X$ together with momentum

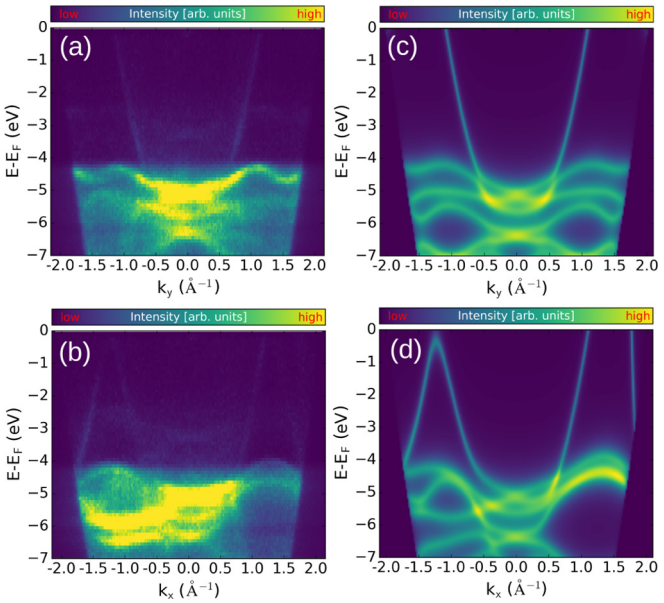

FIG. 9. Ag(111) ARPES data for $\Omega = 21.2$ eV. (a), (b) Experimental data along two different $k_{||}$ directions. (c), (d) Theoretical spectra.

maps (Fig. 10) for a binding energy of -0.5 eV. In terms of energetic positions and dispersion, the agreement between theory and experiment is remarkable even though we made a simple nearly free-electron state approximation for the final state, i.e. neglected resonant band transitions completely and left the dipole matrix elements constant. Figure 10(a) seems to exhibit a similar momentum-dependent band modulation as we have seen in Fig. 7(b), indicating a possible final-state effect.

As a second example, we compare our simulations of Au(111) with experimental data of Courths *et al.* [45] (see Fig. 11). Except for the lowest-lying band, which is not visible in the experimental data, the photon energy dependence, reflecting the k_z dispersion, is predicted very well. With such an analysis, not only the spectral width and dispersion can be extracted from the experiment, but also model parameters such as the spin-orbit coupling parameter or hybridization strengths (entering the combined interpolation scheme).

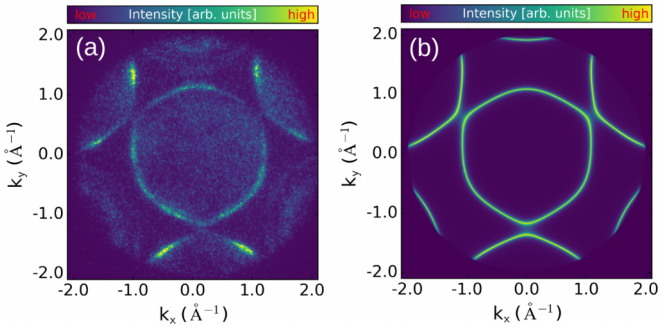

FIG. 10. Experimental (a) and theoretical (b) momentum maps of Ag(111), $\Omega = 21.2$ eV. Sp-band cut at a binding energy $E - E_F = -0.5$ eV.

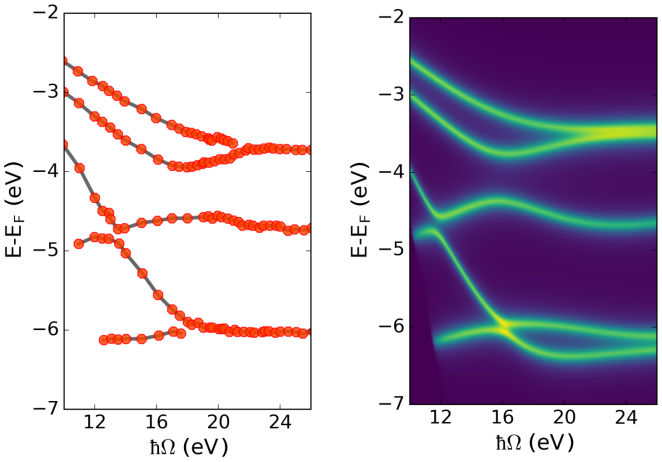

FIG. 11. Photon energy dependence for photoemission from a Au(111) crystal. Left: experimental data for normal photoemission intensity peaks, extracted from [45]. Right: simulation based on the combined-interpolation scheme. ARPES cuts from the Γ point, i.e., $k_{\|} = 0$, are shown as a function of photon energy.

X. SIMULATION GUIDANCE

By now, the paper dealt with a detailed derivation of photoemission formulas, but as we are aiming at giving experimentalists an applicable tool to simulate and analyze their experimental data, we now give a short summary and recipe on how to use the presented theory, for the simple example of bulk photoemission without complex self-energy corrections:

(1) Start with formula (31),

$$j_{\mathrm{pes}}^{\mathrm{bulk}}(\mathbf{k}_{\|}, E) = \sum_n |M_n|^2 A_0^2 \frac{k_v}{|k_{\mathrm{sr}}|} \frac{\theta(E - \varepsilon_{\mathbf{k}_{\|}})}{(k_v + k_{\mathrm{sr}})^2 + k_{\mathrm{si}}^2} \times f(E - \Omega + \Phi) A_n^{\mathrm{bulk}}(\mathbf{k}_{\|}, k_z, E - \Omega)|_{k_z = k_{\mathrm{sr}}}$$

and assume the dipole matrix element M_n to be constant for band n.

(2) In formulas (16), (17), and (18) assume the self-energy to be purely imaginary, i.e.,

$$\Sigma^r(\omega) = i\,\mathrm{Im}\Sigma^r(\omega) = -i\Gamma$$

with a final-state spectral width parameter Γ.

(3) Use the spectral function approximation (43) for the initial state

$$A_n(\mathbf{k}, E) = \frac{2\Gamma}{(E - \varepsilon_{n,\mathbf{k}} + \mu)^2 + \Gamma^2},$$

where Γ is the spectral width of the initial state.

(4) For band n, model the dispersion $\varepsilon_{n,\mathbf{k}}$ either with an analytical function or use a suitable numerical method such as a tight-binding-method, the combined-interpolation scheme or density-functional theory.

XI. LIMITATIONS OF THE MODEL AND FUTURE PROSPECTS

Although the use of nearly free-electron-like final states has been proven to be very useful in the interpretation of photoemission data, it is well known that this picture has its limitations. The effect of resonant band-to-band transitions can lead to the appearance of discontinuous intensity variations and irregularities in the band dispersions in a photoemission spectrum [1]. There are also systems where the final state influences or even dominates the observed dispersive behavior [46]. The neglect of dipole matrix elements dismisses the polarization dependency of the used photon source and symmetry effects of possible initial- and final-state transitions [47,48]. However, a possible disagreement between our proposed method and experimental data can also give valuable information for individual bands when final-state and matrix element effects have to be taken into account. Despite the existence of known shortcomings in the approximations made so far, the method developed here is meant to serve as a starting point for a quantitative interpretation of ARPES spectra with a focus on applicability and speed. Further steps to extend our method and to a better theory could include energy- and momentum-dependent dipole matrix elements which could be already calculated via the combined interpolation scheme [27]. Polarization effects of the used light source could be incorporated with the approximation of Shevchik and Liebowitz [21] by using an atomiclike dipole matrix element approximation, although this would further increase the number of free parameters in the theory.

XII. CONCLUSION

We have presented a versatile basic theoretical formulation of one-photon photoemission for the simulation of ARPES data. The method combines band structure calculations based on the combined interpolation scheme with a perturbation theory formulation of the photoemission process on the Keldysh contour. Our method includes the full momentum, energy, and photon-energy dependency needed to describe an ARPES experiment and predicts measured band dispersions, demonstrated for the noble metals Ag(111) and Au(111), correctly. Analytical formulas have been given, which could be directly used for data fitting and parameter estimation. Our model includes spectral broadening mechanisms related to initial and final states, a finite penetration depth and a finite spectral width of the used light source. The derived set of Feynman rules for CW or laser excitation can be used to construct the final photoemission formulas directly from a Feynman diagram representation of the angle-resolved photoemission process. This will be in particular useful for the derivation of photoemission formulas for higher-order (nonlinear) spectroscopy methods.

ACKNOWLEDGMENTS

This work was supported by the German Science Foundation (DFG) within the SFB/TRR 173 “Spin + X”, Project A02, and SFB 1073, Atomic scale control of energy conversion, Project B07.

[1] H. Wern, R. Courths, G. Leschik, and S. Hüfner, On the band structure of silver and platinum from angle-resolved photoelectron spectroscopy (ARUPS) measurements, Z. Phys. B: Condens. Matter **60**, 293 (1985).

[2] P. Aebi, J. Osterwalder, R. Fasel, D. Naumović, and L. Schlapbach, Fermi surface mapping with photoelectrons at UV energies, Surf. Sci. **307**, 917 (1994).

[3] P. Puschnig, S. Berkebile, A. J. Fleming, G. Koller, K. Emtsev, T. Seyller, J. D. Riley, C. Ambrosch-Draxl, F. P. Netzer, and M. G. Ramsey, Reconstruction of molecular orbital densities from photoemission data, Science **326**, 702 (2009).

[4] A. Damascelli, Z. Hussain, and Z.-X. Shen, Angle-resolved photoemission studies of the cuprate superconductors, Rev. Mod. Phys. **75**, 473 (2003).

[5] T. Cuk, D. H. Lu, X. J. Zhou, Z.-X. Shen, T. P. Devereaux, and N. Nagaosa, A review of electron–phonon coupling seen in the high-T_c superconductors by angle-resolved photoemission studies (ARPES), Phys. Status Solidi B **242**, 11 (2005).

[6] G. Bian, T.-R. Chang, R. Sankar, S.-Y. Xu, H. Zheng, T. Neupert, C.-K. Chiu, S.-M. Huang, G. Chang, I. Belopolski, D. S. Sanchez, M. Neupane, N. Alidoust, C. Liu, B. Wang, C.-C. Lee, H.-T. Jeng, C. Zhang, Z. Yuan, S. Jia *et al.*, Topological nodal-line fermions in spin-orbit metal $PbTaSe_2$, Nat. Commun. **7**, 10556 (2016).

[7] U. De Giovannini, H. Hübener, and A. Rubio, A first-principles time-dependent density functional theory framework for spin and time-resolved angular-resolved photoelectron spectroscopy in periodic systems, J. Chem. Theory Comput. **13**, 265 (2017).

[8] H. Huang and W. Duan, Topological insulators: Quasi-1D topological insulators, Nat. Mater. **15**, 129 (2016).

[9] H. Ebert, D. Ködderitzsch, and J. Minár, Calculating condensed matter properties using the KKR-Green's function method–recent developments and applications, Rep. Prog. Phys. **74**, 096501 (2011).

[10] A. Winkelmann, C. Tusche, A. A. Ünal, M. Ellguth, J. Henk, and J. Kirschner, Analysis of the electronic structure of copper via two-dimensional photoelectron momentum distribution patterns, New J. Phys. **14**, 043009 (2012).

[11] J. Braun, R. Rausch, M. Potthoff, J. Minár, and H. Ebert, One-step theory of pump-probe photoemission, Phys. Rev. B **91**, 035119 (2015).

[12] A. F. Kemper, M. A. Sentef, B. Moritz, T. P. Devereaux, and J. K. Freericks, Review of the theoretical description of time-resolved angle-resolved photoemission spectroscopy in electron-phonon mediated superconductors, Ann. Phys. **529**, 1600235 (2017).

[13] H. Aoki, N. Tsuji, M. Eckstein, M. Kollar, T. Oka, and P. Werner, Nonequilibrium dynamical mean-field theory and its applications, Rev. Mod. Phys. **86**, 779 (2014).

[14] E. Perfetto, D. Sangalli, A. Marini, and G. Stefanucci, First-principles approach to excitons in time-resolved and angle-resolved photoemission spectra, Phys. Rev. B **94**, 245303 (2016).

[15] I. Adawi, Theory of the surface photoelectric effect for one and two photons, Phys. Rev. **134**, A788 (1964).

[16] C. N. Berglund and W. E. Spicer, Photoemission studies of copper and silver: Theory, Phys. Rev. **136**, A1030 (1964).

[17] G. D. Mahan, Theory of photoemission in simple metals, Phys. Rev. B **2**, 4334 (1970).

[18] P. J. Feibelman and D. E. Eastman, Photoemission spectroscopy-correspondence between quantum theory and experimental phenomenology, Phys. Rev. B **10**, 4932 (1974).

[19] W. L. Schaich and N. W. Ashcroft, Theory of photoemission, Solid State Commun. **8**, 1959 (1970).

[20] J. B. Pendry, Theory of photoemission, Surf. Sci. **57**, 679 (1976).

[21] N. J. Shevchik and D. Liebowitz, Theory of angle-resolved photoemission from the bulk bands of solids. I. Formalism, Phys. Rev. B **18**, 1618 (1978).

[22] L. V. Keldysh, Diagram technique for nonequilibrium processes, Zh. Eksp. Teor. Fiz. **47**, 1515 (1964) [Sov. Phys. JETP **20**, 1018 (1965)].

[23] R. A. Craig, Perturbation expansion for real-time Green's functions, J. Math. Phys. **9**, 605 (1968).

[24] M. Bonitz and D. Semkat, *Proceedings of the Conference, Progress in Nonequilibrium Green's Functions, Dresden, Germany, 19-23 August 2002* (World Scientific, Singapore, 2003).

[25] C. Caroli, D. Lederer-Rozenblatt, B. Roulet, and D. Saint-James, Inelastic Effects in Photoemission: Microscopic Formulation and Qualitative Discussion, Phys. Rev. B **8**, 4552 (1973).

[26] N. V. Smith and L. F. Mattheiss, Photoemission spectra and band structures of d-band metals. I. Practical aspects of fcc interpolation schemes, Phys. Rev. B **9**, 1341 (1974).

[27] N. V. Smith, Photoemission spectra and band structures of d-band metals. VII. Extensions of the combined interpolation scheme, Phys. Rev. B **19**, 5019 (1979).

[28] E. Pehlke, W. Schattke, O. Anderson, R. Manzke, and M. Skibowski, Photoemission from the (001) surface of 1T-$TiSe_2$: Comparison of calculation with experiment, Phys. Rev. B **41**, 2982 (1990).

[29] W. L. Schaich and N. W. Ashcroft, Model calculations in the theory of photoemission, Phys. Rev. B **3**, 2452 (1971).

[30] J.-J. Chang and D. C. Langreth, Deep-hole excitations in solids. II. Plasmons and surface effects in x-ray photoemission, Phys. Rev. B **8**, 4638 (1973).

[31] C.-O. Almbladh, On the theory of photoemission, Phys. Scr. **32**, 341 (1985).

[32] H. Keiter, Comment on many-body aspects of external photoemission, Z. Phys. B: Condens. Matter **30**, 167 (1978).

[33] H. Gollisch, D. Meinert, E. Tamura, and R. Feder, Electron-hole scattering in photoemission, Solid state Commun. **82**, 197 (1992).

[34] H. Arai and T. Fujikawa, Single-site and multisite resonant photoemission theory studied by Keldysh Green's functions, Phys. Rev. B **72**, 075102 (2005).

[35] C.-O. Almbladh, Photoemission beyond the sudden approximation, J. Phys.: Conf. Ser. **35**, 127 (2006).

[36] D. C. Langreth and J. W. Wilkins, Theory of spin resonance in dilute magnetic alloys, Phys. Rev. B **6**, 3189 (1972).

[37] D. C. Langreth, Scattering effects in photoelectric emission from solids. I, Phys. Rev. B **3**, 3120 (1971).

[38] F. Roth, T. Arion, H. Kaser, A. Gottwald, and W. Eberhardt, Angle resolved photoemission from Ag and Au single crystals: Final state lifetimes in the attosecond range, J. Electron Spectrosc. Relat. Phenom. **224**, 84 (2018).

[39] S. Eich, A. Stange, A. V. Carr, J. Urbancic, T. Popmintchev, M. Wiesenmayer, K. Jansen, A. Ruffing, S. Jakobs, T. Rohwer *et al.*, Time-and angle-resolved photoemission spectroscopy with optimized high-harmonic pulses using frequency-doubled Ti:Sapphire lasers, J. Electron Spectrosc. Relat. Phenom. **195**, 231 (2014).

[40] W. S. M. Werner, K. Glantschnig, and C. Ambrosch-Draxl, Optical constants and inelastic electron-scattering data for 17 elemental metals, J. Phys. Chem. Ref. Data **38**, 1013 (2009).

[41] G. C. Fletcher, Density of states curve for the 3d electrons in nickel, Proc. Phys. Soc., Sect. A **65**, 192 (1952).

[42] L. Hodges, H. Ehrenreich, and N. D. Lang, Interpolation scheme for band structure of noble and transition metals: Ferromagnetism and neutron diffraction in Ni, Phys. Rev. **152**, 505 (1966).

[43] F. M. Mueller, Combined interpolation scheme for transition and noble metals, Phys. Rev. **153**, 659 (1967).

[44] R. Lässer, N. V. Smith, and R. L. Benbow, Empirical band calculations of the optical properties of *d*-band metals. I. Cu, Ag, and Au, Phys. Rev. B **24**, 1895 (1981).

[45] R. Courths, H. G. Zimmer, A. Goldmann, and H. Saalfeld, Electronic structure of gold: An angle-resolved photoemission study along the Λ line, Phys. Rev. B **34**, 3577 (1986).

[46] X. Gao, A. N. Koveshnikov, R. H. Madjoe, R. L. Stockbauer, and R. L. Kurtz, Dominance of the Final State in Photoemission Mapping of the Fermi Surface of Co/Cu(001), Phys. Rev. Lett. **90**, 037603 (2003).

[47] M. Lindroos, S. Sahrakorpi, and A. Bansil, Matrix element effects in angle-resolved photoemission from $Bi_2Sr_2CaCu_2O_8$: Energy and polarization dependencies, final state spectrum, spectral signatures of specific transitions, and related issues, Phys. Rev. B **65**, 054514 (2002).

[48] R. L. Kurtz, D. A. Browne, and G. J. Mankey, Final state effects in photoemission studies of Fermi surfaces, J. Phys.: Condens. Matter **19**, 355001 (2007).